Potential Application of Tungsten Carbides as Electrocatalysts: 4. Reactions of Methanol, Water, and Carbon Monoxide over Carbide-Modified W(110)

Henry H. Hwu and Jingguang G. Chen*

Center for Catalytic Science and Technology, Department of Materials Science and Engineering, University of Delaware, Newark, Delaware 19716

Received: September 4, 2002; In Final Form: December 13, 2002

The reactions of methanol, water, and carbon monoxide over clean and carbide-modified W(110) are studied by using temperature-programmed desorption, high-resolution electron energy loss spectroscopy, and Auger electron spectroscopy . The product selectivity of methanol on unmodified W(110) is 67.5% toward complete decomposition, 8.5% toward CO, and 24% toward CH_4. After the W(110) surface is modified by carbon, the complete decomposition pathway decreases to 58%, with the remaining methanol dissociating to produce approximately equal amounts of CO and CH_4. On W(110), the number of H_2O molecules undergoing dissociation is determined to be 0.320 water molecules per W atom. Upon carbon modification, the activity of water decreases by half to 0.153 molecules per W atom. The study of CO on W(110) shows three reaction pathways: decomposition to surface C and O, formation of gas-phase CO_2, and molecular desorption at 284 and 335 K. On the C/W(110) surface, only 7% of the adsorbed CO decomposes to produce surface C and O; additionally, no CO_2 desorption is detected. The preadsorption of water onto C/W(110) does not appear to affect the amount of CO adsorption, but does lead to CO desorbing at the lower temperature of 271 K. These results are compared to our previous studies on W(111) and C/W(111) to determine the effect of substrate structure on the reaction pathways of methanol, water, and CO.

1. Introduction

This work is the fourth in a series of papers attempting to evaluate the feasibility of tungsten carbides as fuel cell electrocatalysts. In particular, these studies focus on the fundamental surface science studies of the anodic chemistry of the direct methanol fuel cell (DMFC), where water and methanol are oxidized to produced protons, electrons, and gas-phase CO_2.[1,2] Currently, the most effective electrocatalyst for the DMFC anode is the bimetallic system of Pt/Ru; this material is favored because it demonstrates significant activity for methanol oxidation *as well as* the dehydrogenation of water, which is critical for the removal of adsorbed CO species.[2−5] Aside from its activity, however, the Pt/Ru system is disadvantageous in terms of its high costs, limited supplies, and its susceptibility to CO poisoning.[6] As a result, the discovery of less expensive and more CO tolerant alternatives to the Pt/Ru catalysts would help facilitate the commercialization of the methanol-based fuel cell systems.

The carbides of groups IV−VI early transition metals often show catalytic properties similar to that of the Pt-group metals, especially in hydrogenation and dehydrogenation reactions involving unsaturated hydrocarbons.[7,8] In particular, there have been numerous studies on tungsten carbides (WC and W_2C) since Levy and Boudart[9] suggested that WC displayed Pt-like behavior in a variety of catalytic reactions in 1973. There have also been several attempts to utilize tungsten carbides as an electrocatalyst,[10−15] as it is resistant to acid solutions at anodic potentials.[12,13] However, uncertainties exist concerning whether none, one, or both of the two forms of tungsten carbides are active toward anodic oxidation of methanol.[10] Though some have reported that the catalytic activity of WC is related to the carbon deficiency and oxygen replacement in the carbon layers of the WC lattice,[14,15] no clear evidence has been established.[10]

In part 1 of this series of papers,[16] the decomposition of methanol over clean and carbide-modified W(111), or C/W(111), has been investigated using temperature-programmed desorption (TPD), high-resolution electron energy loss spectroscopy (HREELS), and Auger electron spectroscopy (AES). We found that the C/W(111) surface is active toward the decomposition of methanol, where gas-phase H_2, CO, and CH_4 are detected in addition to surface carbon and oxygen. In part 2 of this investigation,[17] we focused on the decomposition of water and CO over C/W(111). On the C/W(111) surface, the activity toward the decomposition of water is found to be significantly higher than Pt-group metals. For the CO experiments, both molecular and dissociative adsorption are observed on C/W(111). Approximately 10% of the adsorbed CO dissociate, with the rest undergoing reversible desorption at ∼330 K. In addition, coadsorption experiments of water and CO on C/W(111) show that the presence of surface hydroxyls hinders the adsorption of CO and that only a trace amount of gas-phase CO_2 is detected. Compared with Pt and Ru surfaces under similar conditions, these two papers show that the W(111) carbide surface possesses higher activities toward water and methanol decomposition and lower CO desorption temperatures.[16,17]

In the third paper, we described the bonding and reactivity of methanol and water on Pt-modified C/W(111) surfaces.[18] After depositing submonolayer coverages of Pt onto C/W(111), the surface remains active toward the decomposition of methanol but with significantly modified reaction pathways. The presence of the submonolayer Pt prohibits the production of methane, which is an undesirable side product in direct methanol fuel

* Author to whom correspondence should be addressed. E-mail: jgchen@udel.edu.

10.1021/jp0269118 CCC: $25.00
Published on Web 02/11/2003

cells. Furthermore, the Pt-modified C/W(111) surfaces remain active toward the dissociation of water.[18]

Our group has also performed comparative investigations of the reactivities of the C/W(111) and C/W(110) surfaces toward cyclohexene[19,20] and NO.[21,22] In both studies, we found that the C/W(110) surface was less reactive. In addition, we observed that the reaction pathways and product selectivities were different on C/W(110) and C/W(111). On the basis of the results of these investigations, one can conclude that the reactivity of C/W strongly depends on the structure of the substrate. The goal of this work is therefore to examine whether the C/W(110) surface still possesses the desirable properties that were observed for the reactions of CH_3OH, H_2O, and CO on the C/W(111) and Pt-modified C/W(111) surfaces.

2. Experimental Section

2.1. Techniques. The ultra high vacuum (UHV) chamber used in the current study has been described in detail previously.[23] Briefly, it is a three-level stainless steel chamber equipped with AES, low-energy electron diffraction (LEED), and TPD in the top two levels and HREELS in the bottom level. The HREELS spectra reported here were acquired with a primary beam energy of 6 eV. Angles of incidence and reflection were 60° with respect to the surface normal in the specular direction. Count rates in the elastic peak were typically in the range of 4×10^5 to 3×10^6 counts/s, and the spectral resolution was between 40 and 50 cm^{-1} full width at half maximum (fwhm). For TPD experiments the W(110) sample was heated with a linear heating rate of 3 K/s.

The single crystal sample was a [110] oriented, 1.5 mm thick tungsten disk (99.999%), 10 mm in diameter, and was purchased from Metal Crystals and Oxides, Ltd., Cambridge, England. The crystal was spot welded directly to two tantalum posts that serve as electrical connections for resistive heating, as well as thermal contacts for cooling with liquid nitrogen. With this mounting scheme, the temperature of the crystal could be varied between 90 and 1200 K. Methanol (Aldrich, 99+% purity) and deionized water were purified by successive freeze−pump−thaw cycles prior to their use. The purity was verified in situ by mass spectrometry. Oxygen and carbon monoxide were obtained from Matheson (99.99% pure) and were used without further purification. Doses are reported in langmuirs (1 langmuir (L) $= 1 \times 10^{-6}$ Torr · s) and are uncorrected for ion gauge sensitivity. In all experiments, the gas exposures were made at a crystal temperature of 90 K with the crystal located in front of the leak valve. The gas exposures were made by backfilling the vacuum chamber.

2.2. Preparation of Clean and Modified W(110). A clean W(110) crystal surface was prepared by cycles of Ne^+ bombardment at 500 K (sample current ~6 μA) and flashing to 1200 K. These 5 min. cycles were generally repeated three times before annealing at 1200 K for ~5 min. To remove carbon contamination, excess O_2 was used to titrate carbide layers at 1000 K. Oxygen reacted with carbon-covered W(110), which then desorbed as CO at temperatures above 1000 K. This oxygen treatment process was repeated several times to remove both surface and bulk carbon. Auger analysis showed that the C and O impurities were both less than 1% of a monolayer after the above cleaning procedure.

The carbide-modified W(110) surfaces were prepared using ethylene or other unsaturated hydrocarbon molecules as a carbon source, as described previously.[19,23] The carbide surfaces will be referred to as C/W(110). In this work, the carbide surfaces were prepared by exposing W(110) to ethylene at 90 K and then flashed to 1200 K; generally these procedures were repeated for four cycles. The four-cycle C/W(110) surface did not show any overlayer LEED pattern. The Auger C(KLLL 272 eV)/W(MNN 182 eV) ratio was typically between 0.36 and 0.42, which corresponded to an atomic C/W ratio between 0.38 and 0.45, based on standard AES sensitivity factors.[24] Finally, the oxygen-modified W(110) surface, or O/W(110), is made by exposing a clean W(110) surface to 30 lamgmuirs of oxygen at 600 K; the atomic O/W ratio for this surface is approximately 0.8.

3. Results and Interpretations

3.1. Decomposition of Methanol 3.1.1. TPD Results. The TPD spectra from 1.0 langmuir exposure of CH_3OH on W(110) and C/W(110) are compared in Figure 1. On clean W(110), the molecular desorption of methanol occurs at 171 K. The desorption of H_2 is detected at ~417 K, and the evolution of CO and CH_4 is observed at ~403 and 410 K, respectively. At 1084 K, a more intense CO peak is observed (see insert), which is attributed to the recombination of atomic C and O. From comparisons between the relative intensities of this recombinant CO desorption with the low-temperature CO peaks, we conclude that the dominant pathway of methanol on W(110) is the complete decomposition to atomic C and O. After the sample was heated to 1200 K, AES measurements indicate that some atomic oxygen remains on the W(110) surface; this observation, combined with AES data at 600 K, is useful in product selectivity calculations, which will be addressed in the Discussion.

The TPD results of CH_3OH on C/W(110) are qualitatively similar to that on the clean W(110) surface. Methanol desorption occurs at a slightly higher temperature of 190 K. H_2 desorption is observed to be very broad and centered at 384 K. From the mass 16 and 28 spectra, we can identify a CH_4 peak (350−450 K) as well as a CO peak at 403 K. Overall, the TPD results indicate that both the W(110) and C/W(110) surface produce gas-phase methane, carbon monoxide, and hydrogen, but in slightly varying quantities. Last, no detectable amounts of gas-phase formaldehyde, CO_2, or H_2O are detected on either W(110) or C/W(110).

3.1.2. HREELS Results. HREEL spectra following the decomposition of adsorbed CH_3OH on W(110) and C/W(110) are described in this section. The exposures of methanol were made with the crystal temperature at 90 K; the adsorbed layer was then heated to the indicated temperatures and cooled immediately before the HREEL spectra were recorded. Finally, the height of the elastic peaks in all spectra has been normalized to unity, and the expansion factor for each individual spectrum represents the multiplication factor relative to the elastic peak.

For ease of vibrational assignment, multilayer (10 langmuirs) CH_3OH and CD_3OH were adsorbed on an inert oxygen-modified W(110) surface at 90 K, as shown in Figure 2. The relevant peak frequencies are assigned in Table 1. At this exposure, the CH_3OH/O/W(111) layer exhibited the following vibrational features: 758 cm^{-1}, δ(OH); 1042 cm^{-1}, ν(CO); 1143 cm^{-1}, $\gamma(CH_3)$; 1461 cm^{-1}, $\delta(CH_3)$; 2063 cm^{-1}, CO contaminants; 2841 cm^{-1}, $\nu_s(CH_3)$; 2956 cm^{-1}, $\nu_{as}(CH_3)$; and 3267 cm^{-1}, ν-(OH). The relatively weak feature at ~2604 cm^{-1} is likely due to the combination mode from the 1143 and 1461 cm^{-1} features. Additionally, the feature at 2063 cm^{-1} is likely from the adsorption of CO during data acquisition. To facilitate the assignment of vibration features, a comparison of the HREEL spectrum of multilayer CD_3OH on O/W(110) recorded at 90 K is also shown in Figure 2. As expected, frequency shifts are

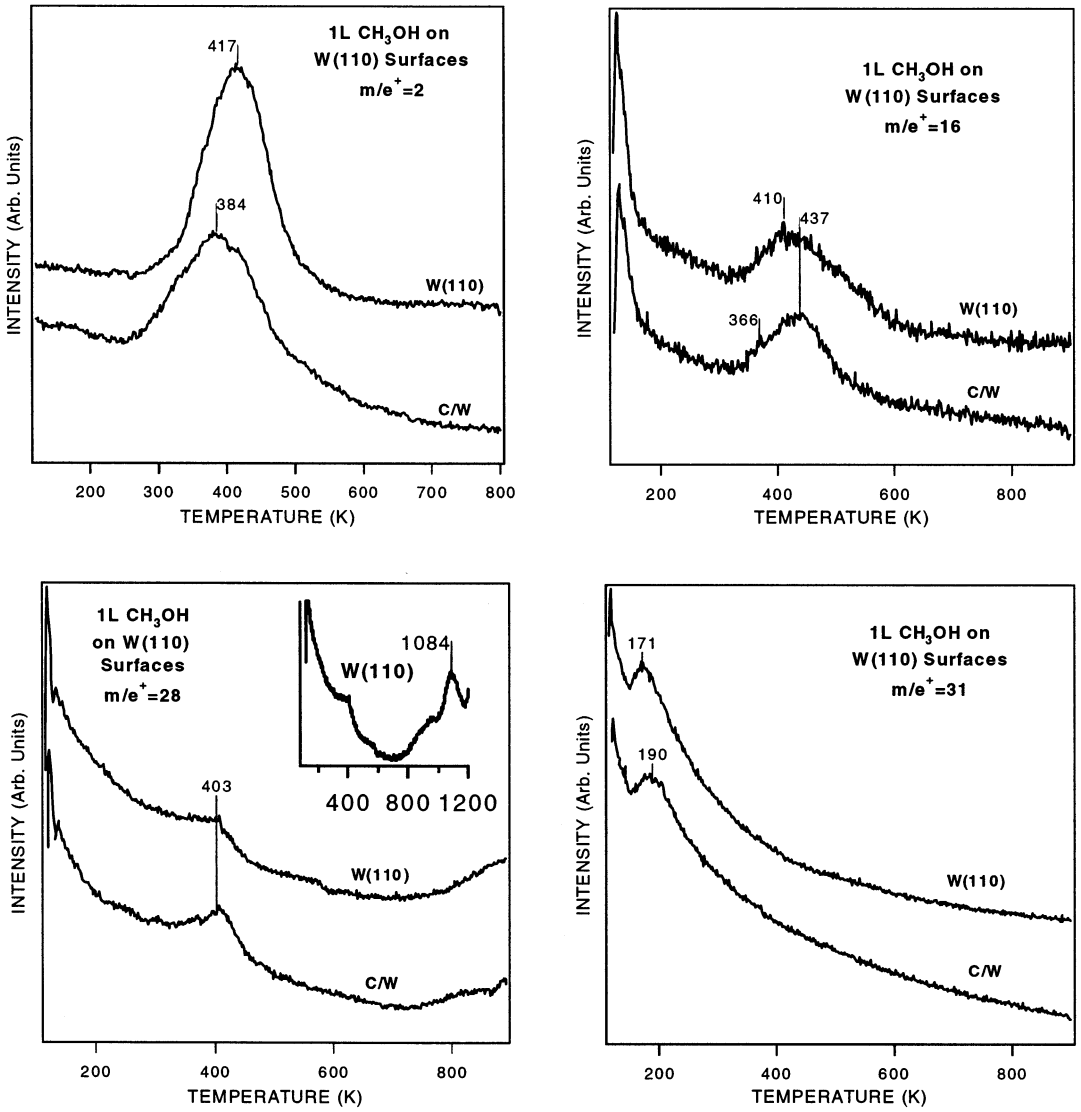

Figure 1. Temperature-programmed desorption spectra of hydrogen, methane, carbon monoxide, and methanol obtained following a 1.0 langmuir exposure of methanol on clean and carbide-modified W(110).

observed for the two vibrational modes involving CH_3 and CD_3 bonds: (1) the $\gamma(CH_3)$ mode shifts from 1143 to 906 cm^{-1}, (2) the $\delta(CH_3)$ mode shifts from 1468 to 1116 cm^{-1}, (3) the ν_s-(CH_3) mode shifts from 2841 to 2090 cm^{-1}, and (4) the ν_{as}-(CH_3) mode shifts from 2956 to 2226 cm^{-1}.

The on-specular spectra recorded after heating the 1.0 langmuirs of CH_3OH/W(110) and CD_3OH/W(110) layers to various temperatures are shown in Figure 3. At 90 K, the vibrational modes of these layers are observed as follows (the frequencies for CD_3OH are in parentheses): 433 (419), 1028 (994), 1157 (900), 1434 (1062), and 2956 (2219) cm^{-1}, as well as a weak CO peak at 1982 cm^{-1}. The relatively weak feature at ~2571 (1955) cm^{-1} is assigned to the combination mode from the 1157 (900) and 1434 (1062) cm^{-1} features. In addition, for the CD_3OH/W(110) layer, the 2056 cm^{-1} peak is assigned to the combination mode from the 994 and 1062 cm^{-1} features. It is important to note the lack of a ν(OH) feature at around 3240 cm^{-1}, which clearly indicates the scission of the methanol OH bond on clean W(110) even at 90 K. The vibrational assignments of the resulting methoxy (CH_3O) species on W(110) and W(111) are summarized in Table 2a. When the layers are heated to 230 K, one cannot discern any significant spectroscopic changes, with the exception of some better-resolved "shouldered peaks". For example, the shouldered peaks at 1277, 1554, and 3076 cm^{-1} can be attributed to the combination modes of the 1157, 1434, and 2956 cm^{-1} modes with a phonon mode shouldering on the elastic peak at ~120 cm^{-1}. In addition, the four weak features between 2151 and 2571 cm^{-1} can all be assigned to a variety of combination modes. Further heating to 330 K again produces no major spectroscopic changes, aside from a slightly more prominent 582 (582) cm^{-1} peak. On the basis of these observations, we can conclude that the majority of the surface methoxy species is formed at 90 K and remains intact until 330 K. When the adsorbed layer is heated to 450 K, the following changes are observed: (1) a decrease in the intensities related to the CH_3 (and CD_3) modes, with the ν(CO) mode shifting to 974 cm^{-1}, and (2) an increase in the intensities of the 609 cm^{-1} mode, which is related to the ν(W−O) mode. By 600 K, nearly all features associated with the methoxy species disappear, and the only features remaining are the W−C and W−O vibrations at 433 (440) and 609 (609) cm^{-1}, respectively.

Figure 4 shows the HREEL spectra of the 1.0 langmuir CH_3-OH/C/W(110) and CD_3OH/C/W(110) layers after heating to higher temperatures. The HREEL spectra at 90 K show features at 1021 (981), 1157 (900), 1448(1069), 1996, 2571 (1941), and 2936 (2212) cm^{-1}. Similar to that observed on clean W(110), the scission of the O−H bond also occurs on C/W(110) at 90 K, as suggested by the absence of a prominent ν(OH) mode at

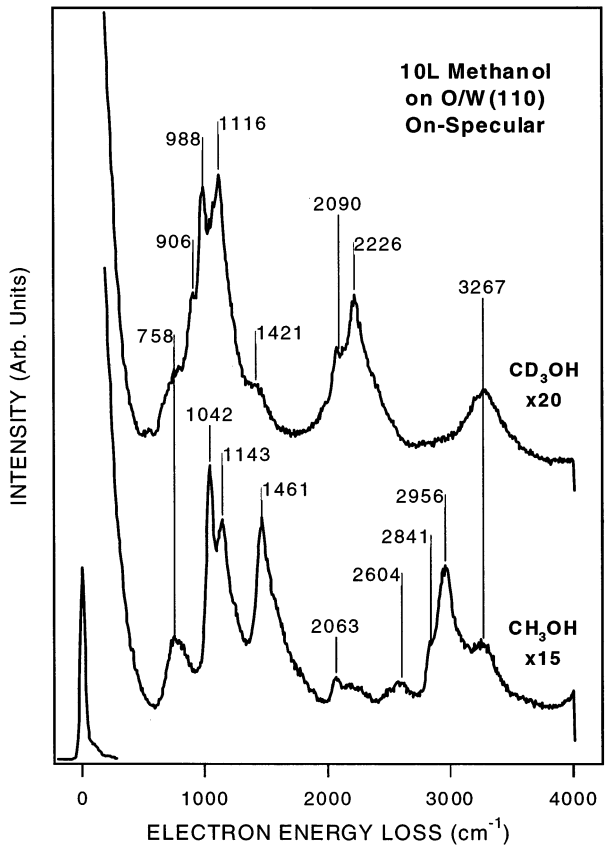

Figure 2. HREEL spectra recorded after exposing oxygen-modified W(110) to 10 langmuir of CH_3OH and CD_3OD at 90 K.

$\sim$3240 cm^{-1}. Similar to that on the clean W(110) surface, modes resulting from the combination of the 1448 cm^{-1} feature and the 120 cm^{-1} phonon mode are observed at 1568 cm^{-1} on C/W(110). When the layers are heated to 230 K, the frequencies of methoxy features remain essentially the same, with an additional peak appearing at 365 cm^{-1} and the ν(CO) mode shifting from 1021 to 994 cm^{-1}. Further heating to 330 K results in no significant spectroscopic changes, with the exception of small features at 521 (501) and 751 (717) cm^{-1}. By 450 K, several significant observations can be made: (1) the intensities of the ν(CO), $\gamma(CH_3)$, $\delta(CH_3)$, and $\nu(CH_3)$ features decrease, with the ν(CO) peak shifting farther from 994 to 974 cm^{-1}, and (2) the ν(W−O) peak at 561 (561) cm^{-1} becomes intense and well-resolved. When the layer is heated to 600 K, the HREEL spectra contain only two modes, 365 (379) and 561 (561) cm^{-1}, which are likely due to the vibrational modes of ν(W−C) and ν(W−O), respectively.

On the basis of the characteristic frequency shifts upon partial deuteration, and by comparison of the corresponding values on Al(111)[25] and W(111),[16] the vibrational features associated with methoxy are summarized in Table 2. In a previous vibrational study of methoxy on Al(111),[25] the ν_H/ν_D ratios of the M−O and C−O modes were reported to be approximately 1.0, because these modes were not affected by the deuteration. For the methyl vibrational features, however, the ν_H/ν_D ratios were $\sim$1.35. Similar isotopic ratios were observed for our previous investigation of methanol on W(111).[16] The results obtained from this work are also very similar to previously published data, as we also observed ν_H/ν_D ratios $\sim$1.0 for the M−O and C−O modes and $\sim$1.35 for the CH_3 modes; these results are summarized in Table 2.

We have also performed off-specular HREELS measurements of methoxy on W(110) and C/W(110) (spectra not shown). These experiments, however, do not reveal any significant variations in the relative intensities of the vibration modes. At this time, we tentatively conclude that the off-specular measurements are incomplete and do not allow for an accurate determination of the methoxy orientation. More studies are currently underway.

3.2. Reactions of Water. 3.2.1. TPD Results. In Figure 5, we show the hydrogen and water TPD spectra obtained after exposing clean W(110) and C/W(110) to 1.0 langmuir of H_2O. From Figure 5, we observe two molecular desorption states at 180 and 198 K from W(110), as well as a hydrogen desorption peak at approximately 402 K. Similar to that on clean W(110), the dissociation of water is also observed on the C/W(110) surface. On the C/W(110) surface, only one molecular desorption peak is found at 178 K. The hydrogen peak is observed at 394 K, and it is significantly weaker in intensity as compared to that from clean W(110).

3.2.2. HREELS Results. The on-specular HREEL spectra of water adsorbed on clean W(110) and C/W(110) surfaces are shown in this section. The exposures of water were made with the crystal temperature at 90 K; the adsorbed layer was then heated to the indicated temperatures and cooled immediately before the HREEL spectra were recorded. Table 3 summarizes the relevant vibrational assignments for these adsorbed layers.

Figure 6 shows the on-specular spectra following the decomposition of 1.0 langmuir of H_2O and D_2O on clean W(110). The following features are observed at 90 K (D_2O frequencies are in parentheses): a weak feature at 433 cm^{-1}, a broad band at 609 (561) cm^{-1}, a peak at 1624 (1197) cm^{-1}, and a broad feature at $\sim$3436 (2557) cm^{-1} with a shoulder at 3680 (2713) cm^{-1}. The two features at 1624 (1197), δ(HOH), and 3436 (2557) cm^{-1}, ν(OH···O), are characteristic of molecular water.[25,26] The 3680 (2713) cm^{-1} feature is related to the ν(OH) of the surface hydroxyl groups; the presence of this vibrational mode indicates that some of the adsorbed molecules begin to dissociate even at 90 K. The remaining features below 1000 cm^{-1} are related to the hindered rotation and $\nu(W-OH_2)$ mode of water at 433 and 609 (561) cm^{-1}, respectively.[25,26] There are essentially no spectroscopic changes when the surface is heated to 140 K, which is consistent with the TPD results. After the sample is heated to 230 K, however, the following changes are observed: (1) the vibrational modes that are related to molecular water completely disappear, (2) the intensity of the surface ν-(OH) feature decreases and shifts to 3538 (2625) cm^{-1}, and (3) well-resolved features are detected at 433 (423) and 602 (602) cm^{-1}. Additionally, one can detect small contamination peaks at 1941 (CO) and $\sim$2940 (CH_x) cm^{-1}.

As discussed in our earlier paper on W(111), the ν(OH) mode of the surface hydroxyl group, produced after the dissociation of H_2O on clean W(111) at 230 K, was relatively sharp and intense.[17] This differs from the HREELS results in Figure 6, which show very weak ν(OH) and ν(OD) modes at 3538 and 2625 cm^{-1}, respectively. This observation suggests that most of the surface hydroxyl groups dissociate on W(110) by 230 K. Recall from the previous TPD section that H_2 desorption does not occur until $\sim$300 K, with the peak center at 402 K. The combined HREELS and TPD results therefore indicate that the evolution of gas-phase hydrogen from W(110) is a desorption-limited process.

It is well known that the ν(metal−H) mode tends to be relatively weak, and its vibrational frequency is often very sensitive to the nature of the surface binding sites. At present, we tentatively assign the feature at 798 cm^{-1} as the ν(W−H) mode. The corresponding ν(W−D) mode should appear at $\sim$570

TABLE 1: Vibrational Frequencies (cm^{-1}) of Solid Phases CH_3OH and CD_3OH, and 10 langmuir CH_3OH and CD_3OH on Oxygen-Modified W(110)

mode	CH_3OH (s)[34]	CD_3OH (s)[34]	ν_H/ν_D	CH_3OH/O/W(110)	CD_3OH/O/W(110)	ν_H/ν_D
δ(OH)	730	708	1.36	758	758	1.00
ν(CO)	1032	983	1.05	1042	988	1.09
$\gamma(CH_3)$	1124	895	1.26	1143	906	1.26
$\delta(CH_3)$	1452	1122	1.29	1461	1116	1.31
$\nu_s(CH_3)$	2828	2075	1.36	2841	2090	1.36
$\nu_{as}(CH_3)$	2951	2213	1.33	2956	2226	1.33
ν(OH)	3225	3195	1.01	3267	3267	1.00

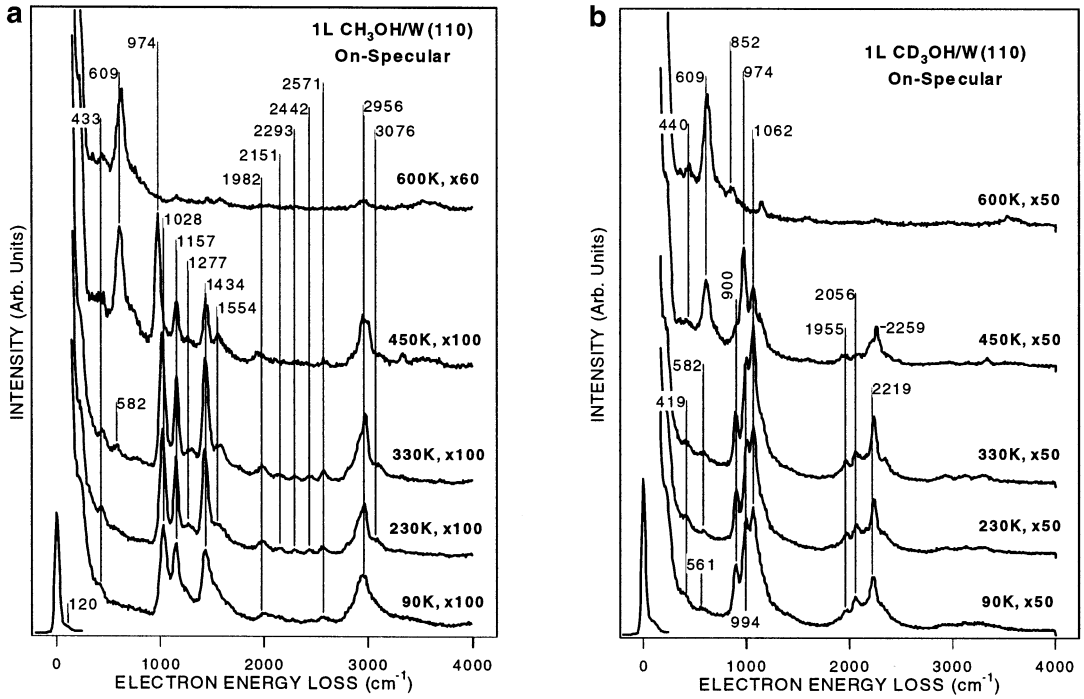

Figure 3. On-specular HREEL spectra which monitor the thermal decomposition of 1.0 langmuir of (a) CH_3OH and (b) CD_3OH on clean W(110) following adsorption at 90 K.

TABLE 2:

(a) Vibrational Frequencies (cm^{-1}) of Methoxy (CH_3O and CD_3O) on Al(111), W(111), and W(110)

mode	$CH_3O(CD_3O)$/Al(111)[25]	ν_H/ν_D	CH_3O/W(111)[16]	$CH_3O(CD_3O)$/W(110)	ν_H/ν_D
ν(M−O)	655 (645)	1.02	467	433 (419)	1.03
ν(CO)	1025 (985)	1.04	1028	1028 (994)	1.03
$\gamma(CH_3)$	1170		1157	1157 (900)	1.29
$\delta(CH_3)$	1475 (1080)	1.37	1461	1434 (1062)	1.35
$\nu_s(CH_3)$	(2065)			(2056)	
$\nu_{as}(CH_3)$	2970 (2235)	1.33	2983	2956 (2219)	1.33

(b) Vibrational Frequencies (cm^{-1}) of Methoxy (CH_3O and CD_3O) on C/W(111) and C/W(110)

mode	$CH_3O(CD_3O)$/C/W(111)[16]	ν_H/ν_D	$CH_3O(CD_3O)$/C/W(110)	ν_H/ν_D
ν(M−O)	534 (487)	1.10	561 (561)	1.00
ν(CO)	1021 (974)	1.05	994 (981)	1.01
$\gamma(CH_3)$	1157 (906)	1.28	1157 (900)	1.29
$\delta(CH_3)$	1448 (1069)	1.35	1448 (1069)	1.35
$\nu_s(CH_3)$	(2063)		(2056)	
$\nu_{as}(CH_3)$	2956 (2226)	1.33	2943 (2212)	1.33

cm^{-1}, which would be masked by the more intense peak at 602 cm^{-1}. Previous HREELS studies of H on W(100) by Ho and co-workers showed that the n(W−H) mode appeared at ~1000 cm^{-1}.[27] The difference between the ν(W−H) frequency in this work and that from H/W(100) is likely due to the different binding environment.

Continuing with the 450 K spectrum in Figure 6a, the ν(W−H) mode at 798 cm^{-1} decreases in intensity, and the spectrum now closely resembles that of the oxygen-modified W(111) surface.[19,23] Additionally, the features at 2185 and 2192 cm^{-1} in Figure 6, parts a and b, respectively, are likely due to the ν(N≡N) vibrations of the adsorbed N_2 from the chamber background.[28] Overall, the HREELS results indicate that water decomposes on clean W(110), producing surface oxygen and eventually gas-phase hydrogen; these observations agree well with the TPD results.

The HREEL spectra obtained for the H_2O/C/W(110) and D_2O/C/W(110) overlayers, shown in Figure 7, are generally similar to those on the clean W(110) surface, with the exception of some differences in relative intensity. At 90 K, water decomposition also begins on the carbide surface, as evidenced by the presence of the 3680 (2713) cm^{-1} ν(OH) feature. The

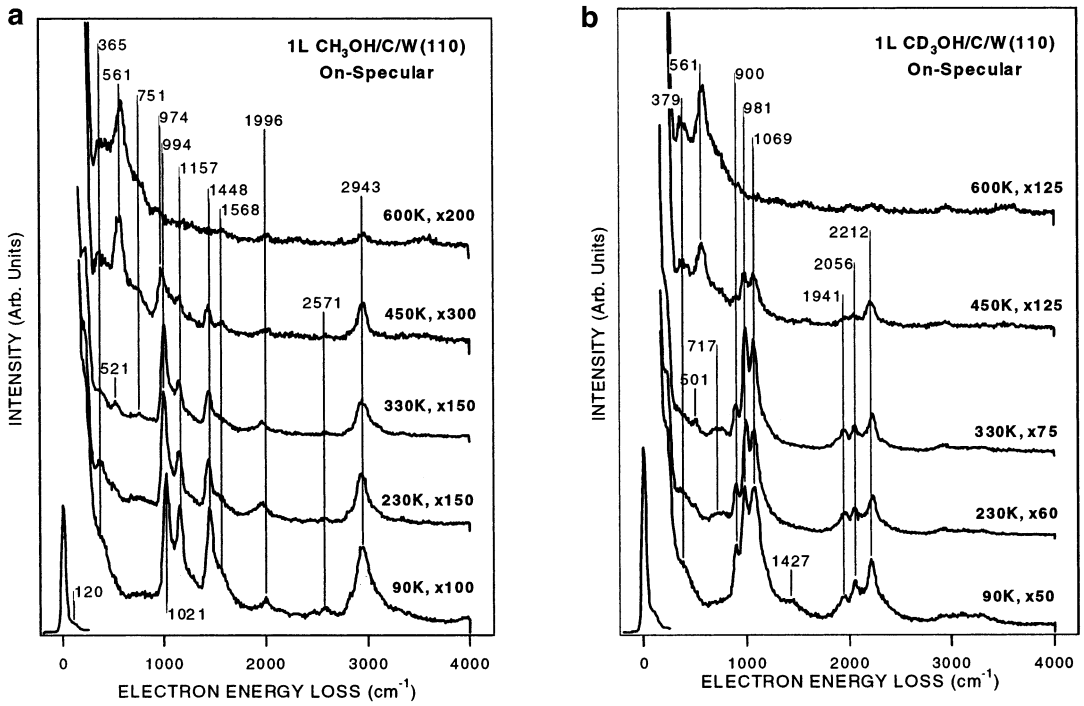

Figure 4. On-specular HREEL spectra which monitor the thermal decomposition of 1.0 langmuir of (a) CH_3OH and (b) CD_3OH on carbide-modified W(110) following adsorption at 90 K.

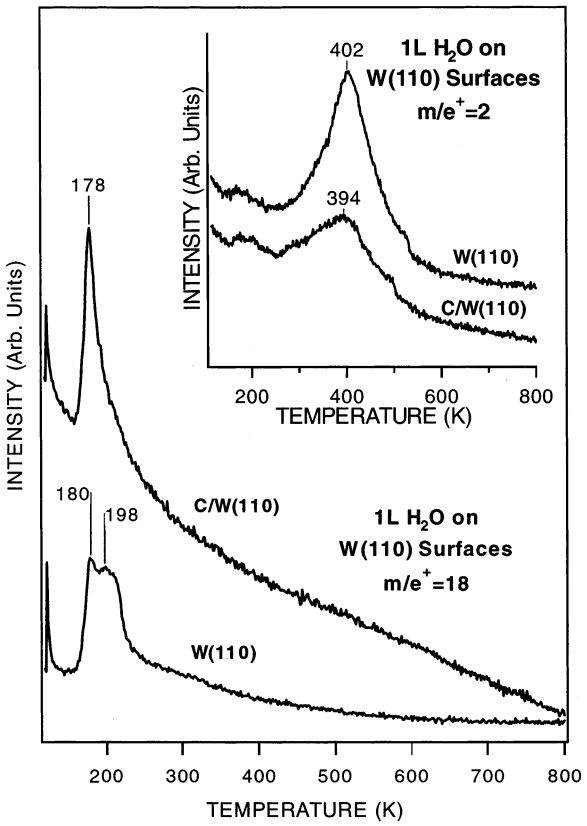

Figure 5. Temperature-programmed desorption spectra of water and hydrogen obtained following a 1.0 langmuir exposure of water on clean and carbide-modified W(110).

other vibrational modes include two peaks at 1630 (1204) and 3470 (2557) cm^{-1} (molecular H_2O), and a broad band at 649 (534) cm^{-1}. The peak positions remain the same after the sample is heated to 140 K. After the sample is heated to 230 K, the molecular H_2O modes disappear, and the only peaks remaining are the two features at 379 (365) and 561 (561) cm^{-1}, a relatively weak ν(OH) feature at 3592 (2652) cm^{-1}, and contamination peaks of CO at 1982 (1948) and of CH_x at 2916 (2929) cm^{-1}. The ν(OH) mode disappears, after heating to 330 K, indicating the complete dissociation of the surface OH groups. Finally, at 450 K, we only observe significant modes at 379 and 561 cm^{-1}, which are indicative of carbide surface with residual oxides on the surface.[16,17,19] Unlike on W(110), we did not detect any well-resolved features that can be assigned to the ν(W−H) or ν(W−D) modes following the dissociation of O−H or O−D groups. More detailed HREEL studies of H_2 or D_2 on C/W(110) are needed to identify these vibrational modes.

TABLE 3: Observed Vibrational Frequencies (cm^{-1}) for Adsorbed Water (D_2O in Parentheses) and Hydroxyl Species

mode	Al(111)[25]	W(111)[17]	C/W(111)[17]	W(110)	C/W(110)
hindered rotations	775 (645)			609 (561)	649 (534)
δ(HOH)	1620 (1210)	1644	1691	1624 (1197)	1630 (1204)
δ(OH)					
ν(HOH)	3450 (2590)	3578	3599	3436 (2557)	3470 (2557)
ν(OH)	3745 (2730)	3687	3748	3680 (2713)	3680 (2713)

3.3. Adsorption and Reactions of CO. Figure 8 shows TPD spectra following the exposure of the W(110) and C/W(110) surfaces to 1.0 langmuir of CO. Both CO and CO_2 are monitored in the TPD experiments. On the clean W(110), most of the CO desorbs molecularly between 200 and 400 K. In addition, a fraction of CO decomposes on W(110), as evidenced by the recombinatory desorption at approximately 1071 K. Monitoring CO_2, one can identify a desorption state at 187 K. On the C/W(110) surface, molecular CO desorbs at 284 and 335 K. Unlike on the clean W(110) surface, the high-temperature recombinatory peak is weaker and broader on C/W(110). Last, the desorption of CO_2 is not detected on the C/W(110) surface.

In addition to CO on W(110) and C/W(110), we also performed measurements involving the coadsorption of water and CO. The preparation of these overlayers is as follows: (1) introduce either low coverage (0.3 langmuir) or saturation coverage (1.0 langmuir) of water on C/W(110) at 90 K, (2) flash

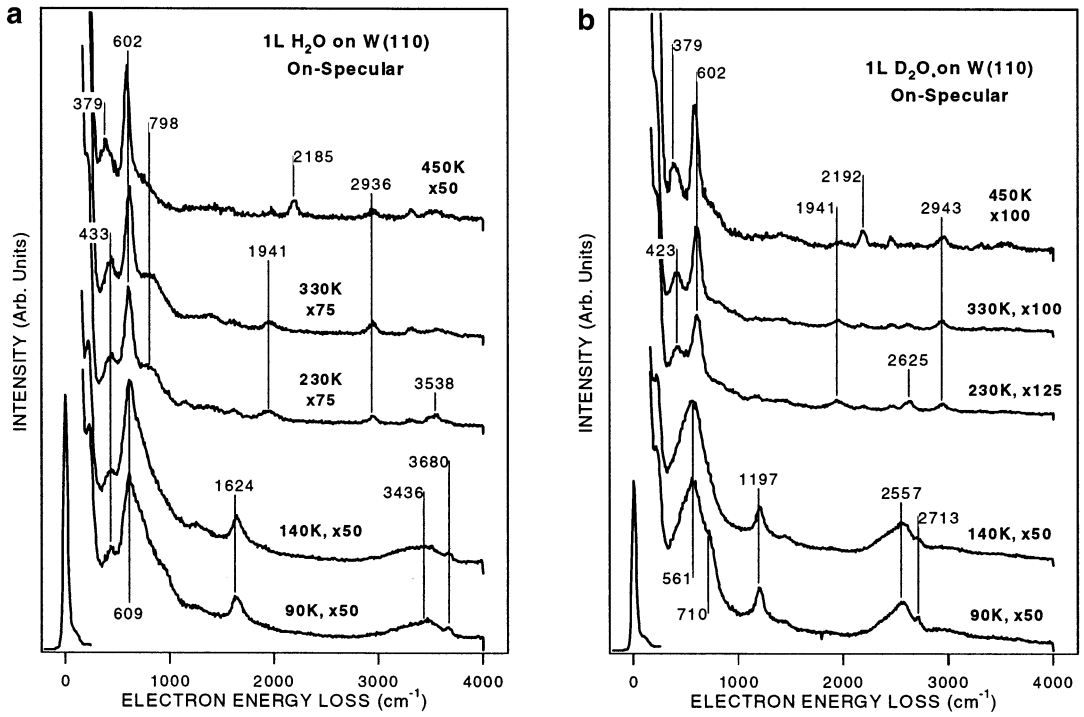

Figure 6. HREEL spectra which monitor the thermal decomposition of 1.0 langmuir (a) H_2O and (b) D_2O on clean W(110) following adsorption at 90 K.

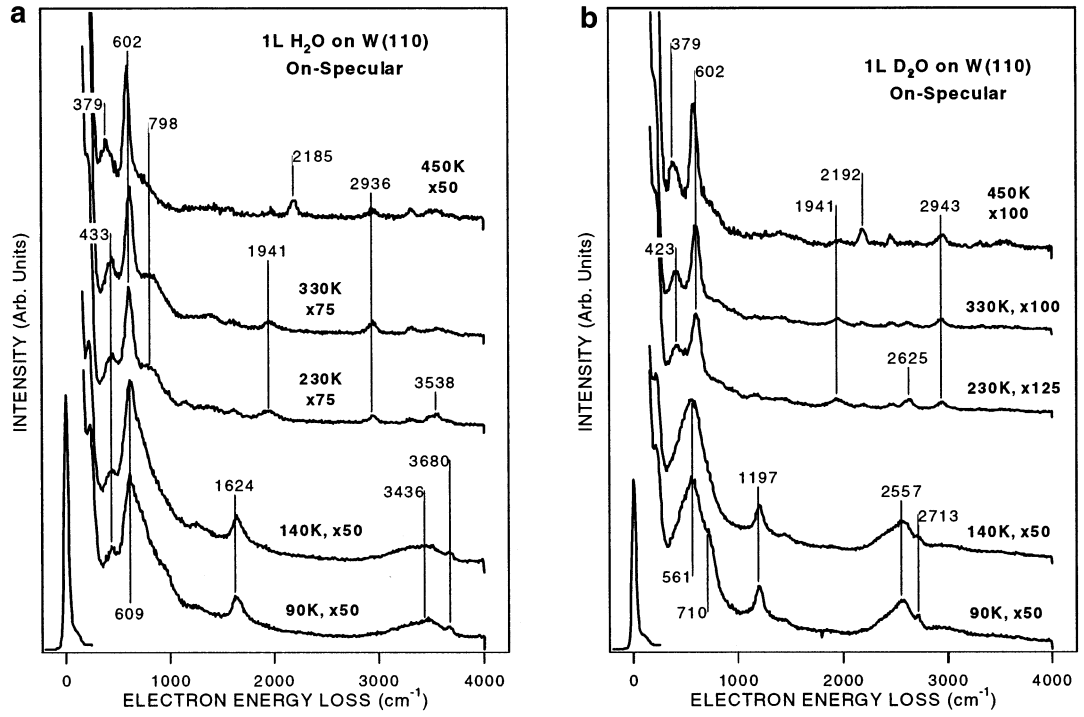

Figure 7. HREEL spectra which monitor the thermal decomposition of 1.0 langmuir (a) H_2O and (b) D_2O on carbide-modified W(110) following adsorption at 90 K.

the H_2O/C/W(110) overlayer to 230 K, and (3) allow the surface to cool to 90 K before exposing the OH/C/W(110) layer to 1.0 langmuir of CO. Referring again to Figure 8, one can see that the presence of water lowers the CO desorption temperature to 271 K. There are also relatively broad and weak CO features found at higher temperatures, which can be attributed to the recombination of C from the surface and O from the decomposed hydroxyl groups. As with the unmodified C/W(110) surface, no CO_2 desorption is found for both low and high water exposures.

Figure 9 shows HREEL spectra following the adsorption of CO on C/W(110) and the 1.0 langmuir H_2O/C/W(110) surfaces, respectively. At 90 K, the ν(CO) and the ν(W−C) modes are observed at 2029 and 352 cm^{-1}, respectively, for C/W(110). In addition, there are two contaminant features at 1448 and 2949 cm^{-1}, which are likely due to the adsorption of background hydrocarbon during HREELS measurements. When the CO/C/W(110) overlayer is heated to 230 K, no major changes are observed, except for the appearance of a shoulder peak at 1908 cm^{-1}. When the layer is heated to 330 K, the 2029 cm^{-1} peak

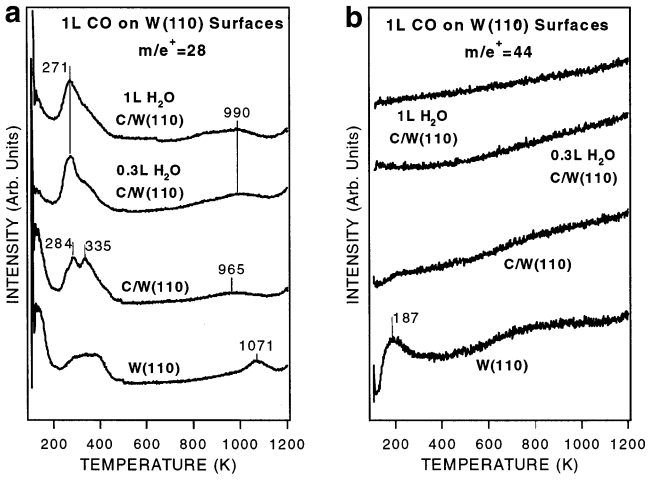

Figure 8. Temperature-programmed desorption spectra of CO and CO_2 obtained following a 1.0 langmuir exposure of CO on clean and carbide-modified W(110), 0.3 langmuir H_2O/C/W(110), and 1.0 langmuir H_2O/C/W(110).

shifts lower to 1908 cm^{-1}, while the 352 cm^{-1} feature shifts higher to 399 cm^{-1}. Further heating to 450 K resulted in the disappearance of the ν(CO) peak and the appearance of a ν-(W−O) mode at 555 cm^{-1}. These spectral changes correspond well with the TPD observations that most of the CO desorbs from the surface by 450 K. The relatively weak feature at 2206 cm^{-1} is likely due to the adsorption of molecular nitrogen from the chamber background.[28] Last, the 600 K spectrum is identical to that at 450 K.

Similar to that observed for the unmodified carbide surface at 90 K, the 1.0 langmuir CO on 1.0 langmuir H_2O/C/W(110) overlayer shows a ν(W−C) mode at 359 cm^{-1}, a ν(CO) mode at 2023 cm^{-1}, and no ν(OH) mode. Heating to 230 K produced almost no spectroscopic changes, aside from the appearance of a 1860 cm^{-1} shoulder peak. Most of the CO desorbs after heating to 330 K, as indicated by the decrease in the intensity of the ν(CO) mode; the energy of this feature also shifts lower to 1969 cm^{-1}. In addition, one can observe two lower energy features at 386 (ν(W−C)) and 548 (ν(W−O)) cm^{-1}. Subsequent heating to temperatures above 450 K resulted in only one spectral change, the disappearance of the ν(CO) mode. Overall, the HREELS results in Figure 9 are consistent with the TPD measurements. Most of the CO molecules desorb molecularly by 450 K, while a fraction of the CO molecules undergo dissociation to atomic C and O, which then recombine to desorb as CO at temperatures above 900 K.

4. Discussion

4.1. Methanol. 4.1.1. Product Yields. On the clean W(110) surface, hydrogen, CH_4, and CO are the gas-phase products, and atomic carbon and oxygen are the remaining surface species after TPD measurements to 600 K. The reaction pathways on W(110) are as follows:

$$x\mathrm{CH_3OH} \xrightarrow{\Delta} x\mathrm{C(a)} + x\mathrm{O(a)} + 2x\mathrm{H_2(g)} \quad (1)$$

$$y\mathrm{CH_3OH} \xrightarrow{\Delta} y\mathrm{CO(g)} + 2y\mathrm{H_2(g)} \quad (2)$$

$$z\mathrm{CH_3OH} \xrightarrow{\Delta} z\mathrm{CH_4(g)} + z\mathrm{O(a)} \quad (3)$$

The value of x in eq 1 can be determined by using AES ratios obtained after TPD experiments to 600 K. At this temperature, AES results reveal a C/W atomic ratio of ∼0.275, or x. Since AES results after heating the CH_3OH/W(110) layer to 1200 K show that no carbon remains on the surface, the C/W ratio of ∼0.275 corresponds to the CO desorption peak at 1084 K in Figure 1. Next, by comparing the areas of the CO peaks at 403 K and at 1084 K peak, we determined that the value of y in eq 2 is ∼0.034. To calculate z from eq 3, we refer back to the AES ratios obtained after TPD experiments to 600 K. As described above, the value x from the atomic C/W ratio at 600 K is ∼0.275; on the other hand, the atomic O/W ratio, or the sum of x and z, is ∼0.373. Using these results, one can estimate z to be 0.098, leading to the following selectivity values:

$$\mathrm{Selectivity}_{\mathrm{CH_4}} \approx \frac{0.098}{(0.098 + 0.275 + 0.034)} \times 100\% = 24\%$$

$$\mathrm{Selectivity}_{\mathrm{CO}} \approx \frac{0.034}{0.407} \times 100\% = 8.5\%$$

$$\mathrm{Selectivity}_{\mathrm{Comp.Decomp.}} \approx \frac{0.275}{0.407} \times 100\% = 67.5\%$$

The dominant reaction pathway (67.5% selectivity) of methanol on clean W(110) is the complete dissociation to form surface carbon, oxygen, and gas-phase hydrogen. The remaining methanol decomposes to CO and hydrogen (8.5%) and to methane and atomic oxygen (24%). Furthermore, the overall activity on the W(110) surface, defined as the total number of CH_3OH undergoing decomposition, is determined to be 0.407 ($x + y + z$) CH_3OH per W atom. As compared in Table 4, it appears that W(110) and W(111) surfaces are very similar in the overall reactivity toward methanol and that they only differ in the selectivities toward the different reaction products.

To estimate the product yields on the C/W(110) surface, one can simply determine the hydrogen and CO TPD peak areas relative to those from W(110). As before, the identical reaction pathways can be written as follows:

$$a\mathrm{CH_3OH} \xrightarrow{\Delta} a\mathrm{C(a)} + a\mathrm{O(a)} + 2a\mathrm{H_2(g)} \quad (4)$$

$$b\mathrm{CH_3OH} \xrightarrow{\Delta} b\mathrm{CO(g)} + 2b\mathrm{H_2(g)} \quad (5)$$

$$c\mathrm{CH_3OH} \xrightarrow{\Delta} c\mathrm{CH_4(g)} + c\mathrm{O(a)} \quad (6)$$

On the basis of TPD data from Figure 1, the following relationships can be used to find a, b, and c:

$$\frac{2(a+b)}{2(x+y)} = \frac{\mathrm{area}_{\mathrm{H_2}}^{\mathrm{C/W(111)}}}{\mathrm{area}_{\mathrm{H_2}}^{\mathrm{W(111)}}} \approx 0.764 \Rightarrow a + b = 0.236 \quad (7)$$

$$\frac{b}{y} = \frac{\mathrm{area}_{\mathrm{CO}}^{\mathrm{C/W(111)}}}{\mathrm{area}_{\mathrm{CO}}^{\mathrm{W(111)}}}[\text{ at temp } < 600\text{ K}] \approx 1.76 \Rightarrow b = 0.060 \quad (8)$$

$$\frac{c}{z} = \frac{\mathrm{area}_{\mathrm{CH_4}}^{\mathrm{C/W(111)}}}{\mathrm{area}_{\mathrm{CH_4}}^{\mathrm{W(111)}}} \approx 0.69 \Rightarrow c = 0.068 \quad (9)$$

From eqs 7−9, we then determine that $a + b + c$ equals 0.304 and that ∼58% of the methanol completely decomposes, while 20% and 22% react to produce gas-phase CO and CH_4,

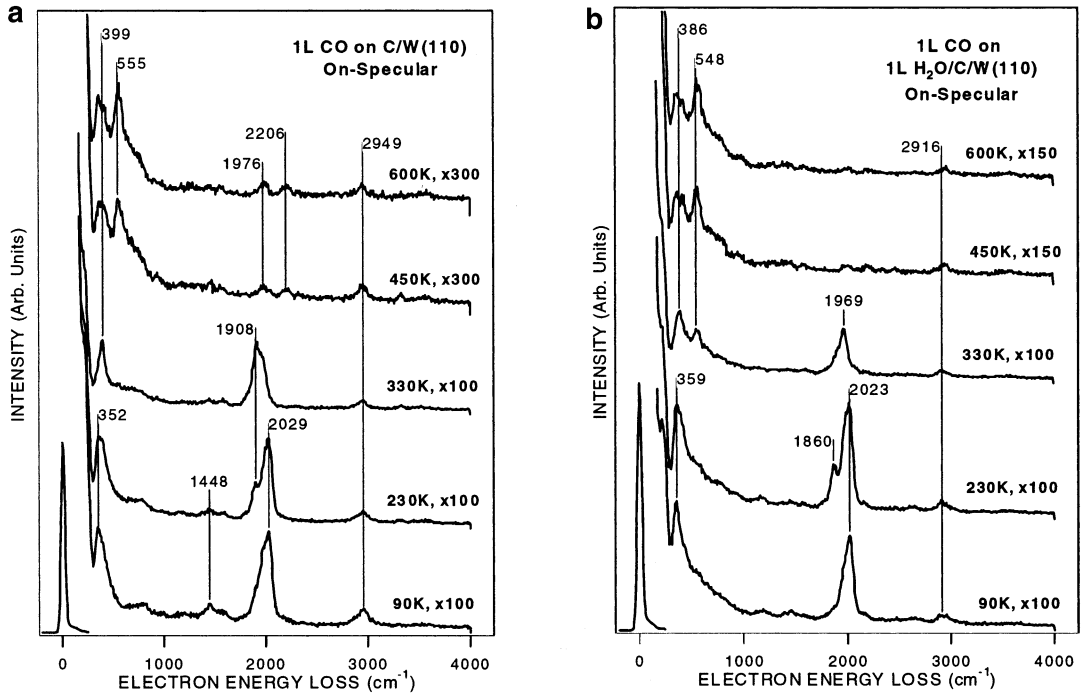

Figure 9. HREEL spectra which monitor the thermal decomposition of 1.0 langmuir CO on (a) C/W(110) and (b) 1.0 langmuir H_2O/C/W(111) following adsorption at 90 K.

TABLE 4: Comparisons of the Product Yields of Methanol on W(111), W(110), C/W(111), and C/W(110) Surfaces

surfaces	complete decompn activ per W atom (%)	CO activity per W atom (%)	CH_4 activity per W atom (%)	total no. of CH_3OH reacting per W atom
clean W(111)[16]	0.350 (85)	0.048 (12)	0.013 (3)	0.411
clean W(110)	0.275 (67.5)	0.034 (8.5)	0.098 (24)	0.407
C/W(111)[16]	0.155 (55)	0.087 (31)	0.038 (14)	0.280
C/W(110)	0.176 (58)	0.060 (20)	0.068 (22)	0.304

TABLE 5: Activities of W(111), W(110), C/W(111), and C/W(110) toward Decomposition of Water

surfaces	activity (water mol per W atom)	% decompn relative to clean W(110) or W(111)
W(111)[17]	0.320	100
W(110)	0.320	100
C/W(111)[17]	0.180	55
C/W(110)	0.153	48

respectively. A summary of the above analysis is also included in Table 4.

4.2. Reaction Pathways of H_2O. Aside from molecular desorption, the only products detected after exposing water to clean W(110) and C/W(110) are gas-phase hydrogen and surface oxygen. After TPD measurements of H_2O on W(110), we obtained an atomic O/W ratio of ~0.32 from AES. The activity of water decomposition on clean W(110) is therefore ~0.32 H_2O molecules per W atom. Next, by comparing the H_2 peak area of C/W(110) to that of clean W(110), we obtain the activity of water dissociation on C/W(110) to be 0.153 molecules per W atom. On the basis of these results, we can conclude that while both surfaces remain active, modifying the W(110) surface with carbon significantly reduces its activity toward the dissociation of water. The activities of H_2O on W(110) and C/W(110) are compared with those on W(111) and C/W(111) in Table 5.

4.3. Decomposition and Reaction of CO. The reaction pathways of CO on the two surfaces are very straightforward: (1) molecular adsorption and desorption, (2) dissociation into surface C and O, which recombines to desorb as CO at high temperatures, and (3) formation of CO_2:

$$\mathrm{CO(ads)} \xrightarrow{\Delta} \mathrm{CO(g)}$$

$$\mathrm{CO(ads)} \xrightarrow{\Delta} \mathrm{C(ads)} + \mathrm{O(ads)} \xrightarrow{\Delta} \mathrm{CO(g)}$$

$$2\mathrm{CO(ads)} \xrightarrow{\Delta} \mathrm{C(ads)} + \mathrm{CO_2(g)}$$

or

$$\mathrm{CO(ads)} + \mathrm{O(ads)} \xrightarrow{\Delta} \mathrm{CO_2(g)}$$

To determine the selectivity toward each pathway, we relied on the results obtained from the methanol studies. In section 4.1.1, we were able to determine the amount of CO desorption from the decomposition of methanol on a per W atom basis. By comparing the CO desorption peak in Figure 8a to that from the decomposition of methanol, we estimate that the TPD areas of the broad low-temperature peak and the 1071 K peak correspond to 0.150 and 0.047 CO molecules per W atom, respectively. TPD measurements also revealed that some CO may have reacted with another CO or surface oxygen to desorb CO_2 at ~187 K. By performing a comparison the TPD peak areas without account for ion gauge sensitivity factors, one can determine that the ratio $\mathrm{area_{CO_2}/area_{CO_{LowT}}}$ is approximately ~0.14. However, the exact yield for the gas-phase CO_2 production cannot be quantified at this time.

We then compared the peak areas of CO desorption from the C/W(110) surface to those from the clean W(110) surface.

TABLE 6: Activities of Clean and Modified C/W(111) and C/W(110) Toward Decomposition of CO

surfaces	mol desorption: CO per W atom (%)	recomb desorption: CO per W atom (%)
C/W(111)[17]	0.103 (90)	0.012 (10)
C/W(110)	0.246 (93)	0.018 (7)
0.3 langmuir H_2O on C/W(111)[17]	0.056	n/a
0.3 langmuir H_2O on C/W(110)	0.252	n/a
1 langmuir H_2O on C/W(111)[17]	0.019	n/a
1 langmuir H_2O on C/W(110)	0.227	n/a

Such a comparison reveals that on C/W(110), only 0.018 CO molecules per W atom (~7%) dissociate into atomic O and C and nearly 93% of the CO molecules (0.246 molecules per W atom) desorb molecularly.

In this study, we also examined the effects of preadsorbing water before introducing CO onto the C/W(110) surface. By comparing the TPD peak areas of the coadsorbed overlayers with that of CO on unmodified C/W(110), we estimate that the amount of low-temperature CO desorption is not very sensitive toward the preexposure of H_2O, with the exception of a reduction in desorption temperature. For the 0.3 langmuir H_2O/1.0 langmuir CO on C/W(110), the amount of CO desorption at 271 K is about the same as that on the surface without water (0.252 CO molecules per W atom). When H_2O exposure is increased to 1.0 langmuir, the CO desorption at 271 K remains at ~92% (0.227 CO molecules per W atom). Because the C/W(110) surface is modified with water before CO exposure, it is uncertain whether the high-temperature recombinant CO feature is from decomposed water reacting with the carbide surface or from the dissociation of adsorbed CO. The calculations presented in this section are summarized in Table 6.

4.4. Comparison with Previous Results on W(111) and W(100) Surfaces. As summarized in Table 4, the degrees of methanol decomposition on clean W(110) and C/W(110) are similar to that on the W(111) and C/W(111) surfaces. On both clean surfaces, approximately 0.4 methanol molecules per W atom react to yield surface carbon and oxygen and gas-phase products of hydrogen, CO, and CH_4. Upon carbon modification, both the C/W(111) and C/W(110) surfaces exhibit some activity reduction toward methanol. The different crystal planes do show variations in product selectivity, however. In the case of the clean surfaces, methanol on W(110) reacts to form significantly more gas-phase CH_4 and slightly less complete decomposition than on W(111). Furthermore, although both C/W(110) and C/W(111) surfaces show ~55% selectivity toward complete decomposition, the C/W(110) surface yields nearly identical amounts of CO (20%) and CH_4 (22%), while the C/W(111) surface produced more CO (31%) than CH_4 (14%).[16]

It is important to point out an interesting difference from the HREELS results of the decomposition of methoxy on C/W(110) and C/W(111). In our previous study on the C/W(111) surface, we observed from HREELS experiments that the ν(C−O) mode of methoxy shifted to a higher frequency when heated to higher temperatures.[16] Following the explanations provided by Hrbek et al.,[29] we suggested that the frequency shift was related to a thermally induced change in the orientation of methoxy to a more perpendicular orientation, leading to a weaker interaction between the CH_3 group with the surface and a stronger (C−O) bond in the methoxy. In contrast, when the sample is heated, the ν(C−O) mode on C/W(110) shifts in the opposite direction (from 1021 to 974 cm^{-1}). By application of the same arguments, the frequency shift suggests that the CO bond of methoxy becomes weaker, most likely due to a stronger interaction between the CH_3 group of the methoxy and the C/W(110) surface at higher temperatures.

The interactions of methanol with W(100) and C/W(100) have previously been investigated by Madix and co-workers.[30] In general, the reaction pathways and product distributions on W(100) are very similar to that observed on W(110) and W(111), with the exception that formaldehyde is formed on the W(100) surface.[16,30] The carbide surface of W(100) is different from the C/W(110) and C/W(111) surfaces, in that it did not completely decompose methanol.[30] Overall, however, methanol activities on these three tungsten crystal planes appear to be relatively structure insensitive. On the other hand, the product selectivities are certainly structure sensitive.

Similar to the reaction of methanol, the reaction of water appears to be relatively structure insensitive. Both clean W(111) and W(110) exhibited a surface activity of 0.32 molecules per W atom. Upon carbide modification, both surfaces showed approximately 50% reduction in the activity toward water dissociation. One difference between the two planes is the desorption temperature and peak shape of H_2. On the (110) plane, a single desorption peak occurs ~400 K for both the W(110) and C/W(110); in contrast, hydrogen desorbs at lower temperatures and with multiple desorption states on the (111) plane.[17] Although both C/W(111) and C/W(110) show activity toward the dissociation of water at 90 K (as evidenced by the presence of the ν(OH) mode from HREELS experiments), the vibrations associated with surface OH groups essentially disappear by 230 K on C/W(110) but were still observed on C/W(111) at this temperature.[17]

In addition to our previous investigation of CO on C/W(111),[17] the chemistry of CO on C/W(100) has also been extensively studied.[31−33] On both clean W(111) and W(100), a saturation exposure of CO resulted in a molecular desorption feature below 400 K and a recombinatory peak at temperatures above 850 K. CO on W(110) behaves the same, with a CO desorption between 200 and 400 K, followed by a 1071 K peak. For all three crystal planes, carbide modification leads to a significant reduction in the dissociation of CO; in particular, the CO dissociation channel is completely suppressed for the W(100)−(5 × 1)C surface.[31] In our studies, we also examined the effect of water modification on the CO activity of C/W(110) and C/W(111). For C/W(111), the preexposures of water resulted in significantly less CO adsorbing onto the surface.[17] Surprisingly, identical experiments on C/W(110) showed that CO adsorption is unaffected by the presence of OH groups. For both C/W(110) and C/W(111), however, the presence of water leads to the decrease of the molecular desorption temperatures. Furthermore, the adsorption of water did not induce the formation of CO_2 on either C/W(110) or C/W(111).

5. Conclusions

This study provides a comparison for our previous reports of CH_3OH, H_2O, and CO on W(111) and C/W(111) surfaces. As before, three reaction pathways were identified following the decomposition of methanol on W(110) and C/W(110): production of methane and atomic oxygen, production of CO gas-phase hydrogen, and complete decomposition. The overall activity toward methanol decomposition is very similar between the two tungsten planes. The product distributions, however, appear to be structure sensitive. As with the case of methanol, the dissociation activities of water on the W(110) surfaces are also similar to that on the W(111) surfaces. CO desorption on

C/W(110) is observed at 284 and 335 K. After this surface is modified with water, however, the desorption temperature is reduced to 271 K. Unlike that on C/W(111), the adsorption of water on C/W(110) does not decrease the amount of CO adsorbed onto the surface.

Similar to the desirable characteristics observed on C/W(111), the C/W(110) surface demonstrates favorable activities that are prerequisite for fuel cell electrocatalysts: the ability to dissociate methanol and water and the desorption of CO at relatively low temperatures. The CO desorption temperature can be further reduced to below room temperature with the preadsorption of water. As a result, the current study further confirms the feasibility for potential application of tungsten carbides as electrocatalysts.

Acknowledgment. We acknowledge financial support from the Basic Energy Sciences of the Department of Energy (DOE/BES Grant No. DE-FG02-00ER15014). H.H.H. also acknowledges financial support from the University of Delaware Presidential Fellowship and the American Vacuum Society Graduate Student Fellowship.

References and Notes

(1) Hamnett, A. *Catal. Today* **1997**, *38*, 445.
(2) Parsons, R.; VanderNoot, T. *J. Electroanal. Chem.* **1988**, *257*, 9.
(3) Hamnett, A.; Kennedy, B. J. *Electrochim. Acta* **1988**, *33*, 1613.
(4) Janssen, M. M. P.; Moolhuysen, J. *Electrochim. Acta* **1976**, *21*, 869.
(5) Campbell, S. A.; Parsons, R. *J. Chem. Soc., Faraday Trans.* **1992**, *88*, 833.
(6) Stonehart, P. In *Electrochemistry and Clean Energy*, Drake, J., Ed.; Royal Society of Chemistry: Cambridge, 1994.
(7) Oyama, S. T. In *The Chemistry of Transition Metal Carbides and Nitrides*; Blackie Academic and Professional: Glasgow, 1996.
(8) Chen, J. G. *Chem. Rev.* **1996**, *96*, 1477.
(9) Levy, R.; Boudart, M. *Science* **1973**, *181*, 547.
(10) Okamoto, H.; Kawamura, G.; Ishikawa, A.; Kudo, T. *J. Electrochem. Soc.* **1987**, *134*, 1645.
(11) Kawamura, G.; Okamoto, H.; Ishikawa, A.; Kudo, T. *J. Electrochem. Soc.* **1987**, *134*, 1653.
(12) Boehm, H.; Pohl, F. A. *Wiss. Ber. AEG-Telefunken* **1968**, *41*, 46.
(13) Binder, H.; Koehling, A.; Sandstede, G. *Am. Chem. Soc. Div. Fuel Chem. Prepr.* **1969**, *13*, 99.
(14) Fleischmann, R.; Boehm, H. *Ber. Bunsen-Ges., Phys. Chem.* **1980**, *84*, 1023.
(15) Ross, P. N., Jr.; Stonehart, P. *J. Catal.* **1977**, *48*, 42.
(16) Hwu, H. H.; Chen, J. G.; Kourtakis, K.; Lavin, J. G. *J. Phys. Chem. B* **2001**, *105*, 10037.
(17) Hwu, H. H.; Polizzotti, B. D.; Chen, J. G. *J. Phys. Chem. B* **2001**, *105*, 10051.
(18) Liu, N.; Rykov, S.; Chen, J. G. *J. Catal.*, in press.
(19) Liu, N.; Rykov, S. A.; Hwu, H. H.; Buelow, M. T.; Chen, J. G. *J. Phys. Chem. B* **2001**, *105*, 3894.
(20) Polizzotti, B. D.; Hwu, H. H.; Chen, J. G. *Surf. Sci.* **2002**, *520*, 97.
(21) Zhang, M. H. et al. *Catal. Lett.* **2001**, *77*, 29.
(22) Zhang, M. H. et al. *Surf. Sci.* **2003**, *522*, 112.
(23) Fruhberger, B.; Chen, J. G. *J. Am. Chem. Soc.* **1996**, *118*, 11599.
(24) Childs, K. D. et al. In *Handbook of Auger Electron Spectroscopy*, #rd ed.; Physical Electronics, Industries: Eden Prairie, MN, 1995.
(25) Chen, J. G.; Basu, P.; Ng, L.; Yates, J. T., Jr. *Surf. Sci.* **1988**, *194*, 397.
(26) Crowell, J. E.; Chen, J. G.; Hercules, D. M.; Yates, J. T., Jr. *J. Chem. Phys.* **1987**, *86*, 5804.
(27) Ho, W.; Willis, R. F.; Plummer, E. W. *Phys. Rev. Lett.* **1978**, *40*, 1463.
(28) Anton, A. B.; Avery, N. R.; Madey, T. E.; Weinberg, W. H. *J. Chem. Phys.* **1986**, *85*, 507. de Paola, R. A.; Hoffmann, F. M.; Heskett, D.; Plummer, E. W. *Phys. Rev. B* **1987**, *35*, 4236.
(29) Hrbek, J.; de Paola, R. A.; Hoffman, F. M. *J. Chem. Phys.* **1984**, *81*, 2818.
(30) Ko, E. I.; Benziger, J. B.; Madix, R. J. *J. Catal.* **1980**, *62*, 264.
(31) Benziger, J. B.; Ko, E. I.; Madix, R. J. *J. Catal.* **1978**, *54*, 514.
(32) Friend, C. M.; Stevens, P. A.; Serafin, J. G.; Baldwin, E. K.; Madix, R. J. *J. Chem. Phys.* **1987**, *87*, 1847.
(33) Stevens, P. A.; Friend, C. M.; Madix, R. J. *Surf. Sci.* **1988**, *205*, 187.
(34) Falk, M.; Whalley, E. *J. Chem. Phys.* **1961**, *34*, 1554.